The Astrophysical Journal, 642:230–243, 2006 May 1

PARALLEL AND PERPENDICULAR TRANSPORT OF HELIOSPHERIC COSMIC RAYS IN AN IMPROVED DYNAMICAL TURBULENCE MODEL

A. Shalchi,[1] J. W. Bieber,[2] W. H. Matthaeus,[2] and R. Schlickeiser[1]
Received 2005 October 26; accepted 2005 December 26

ABSTRACT

By applying a new model for the dynamical magnetic turbulence, we calculate parallel and perpendicular mean free paths of heliospheric cosmic rays. The results are compared with different observations and previous theoretical calculations. It is the main conclusion of this paper that we can achieve agreement between theory and observations if we employ realistic turbulence parameters. Motivated by previous work, we also discuss nonlinear effects in cosmic-ray transport theory.

Subject heading: cosmic rays — diffusion — turbulence

1. INTRODUCTION

The understanding of the interaction between cosmic rays and turbulent electromagnetic fields is one of the fundamental problems of astrophysics. Of particular interest is the diffusion tensor for particle transport parallel and perpendicular to the ordered magnetic field, which controls, e.g., the penetration and modulation of low-energy cosmic rays in the heliosphere, the confinement and escape of Galactic cosmic rays from the Galaxy, and the efficiency of diffusive shock acceleration mechanisms. In axisymmetric turbulence, only the parallel and the perpendicular mean free paths must be known to achieve a full description of spatial transport of cosmic rays.

An early treatment of particle transport employed the quasi-linear theory (QLT; Jokipii 1966) for a simple magnetostatic slab model. Palmer (1982) compared the predictions of this model for the parallel mean free path with heliospheric observations and noted two major problems:

1. Magnitude problem: the observed parallel mean free paths are typically much larger than the predicted QLT results.
2. Flatness problem: the observed parallel mean free paths are generally constant with a rigidity-independent mean free path for 0.5–5000 MV, but QLT predicts that the mean free path should increase with increasing rigidity ($\lambda_{\parallel} \sim R^{1/3}$).

Bieber et al. (1994) suggested a composite slab/two-dimensional model in dynamical turbulence to achieve agreement between theory and observations. Bieber et al. (1994) used the so-called damping model of dynamical turbulence (DT model), where the dynamical correlation function is an exponential function with a simple approximation for the correlation timescale. Although the agreement between this model and observations is acceptable (see also Dröge 2000), there are several unanswered questions. First the DT model applied in Bieber et al. (1994) and Dröge (2000) is a simple model of the interactions responsible for the temporal decorrelation and can be seen as a crude approximation. Furthermore, the DT model does not take into account the plasma wave character of the turbulence. The third problem is the most difficult problem: it was demonstrated in test particle simulations (e.g., Qin et al. 2002a, 2002b) and in several theoretical considerations (e.g., Völk 1973; Shalchi et al. 2004b; Shalchi 2005b; Qin et al. 2005) that nonlinear effects play a crucial role if diffusion coefficients are calculated.

In this paper we revisit the Palmer consensus by considering a more modern turbulence model to describe dynamical turbulence and plasma wave propagation effects. We call this model the nonlinear anisotropic dynamical turbulence (NADT) model, which is explained in § 2.2. It is the purpose of this paper to compute scattering mean free paths in the NADT model and to compare theoretical results of the NADT model with other models and heliospheric observations. The new model, which could be seen as an improvement of the DT model, also contains the plasma wave character of the turbulence.

Besides the parallel mean free path, the mean free path perpendicular to the magnetic background field can also be obtained from observations (e.g., Palmer 1982). For a long time perpendicular diffusion was considered an unsolved problem of particle astrophysics. Previous approaches like the application of QLT (Jokipii 1966; field line random walk limit) or the BAM model (Bieber & Matthaeus 1997) failed to reproduce simulated perpendicular diffusion coefficients (Giacalone & Jokipii 1999; Qin et al. 2002a, 2002b). Recent analyses such as the compound-diffusion model (Kóta & Jokipii 2000) and the direct investigation of the equations of motion (Shalchi 2005a) were able to describe subdiffusion in the slab model, but they cannot describe the recovery of diffusion in nonslab models. Only the recently derived nonlinear guiding center theory (NLGC theory; Matthaeus et al. 2003) and the weakly nonlinear theory (WNLT; Shalchi et al. 2004b), which can be understood as a unification of NGLC theory and QLT, can reproduce the simulated diffusion coefficients. In the current paper we employ the NLGC approach because this theory is more tractable than WNLT. Although NLGC theory is different from the QLT approach, it allows a straightforward calculation of the perpendicular mean free path.

Because of recent test particle simulations (Qin et al. 2002a, 2002b, 2005) and theoretical considerations (Shalchi et al. 2004b), we expect that nonlinear effects are also important for parallel transport if a nonslab model is assumed. Furthermore, it has been known since the early 1970s (e.g., Völk 1973) that magnetostatic QLT is invalid for pitch-angle scattering close to 90°. Thus, the importance of nonlinear effects is discussed throughout the whole paper.

In § 2 we present the NADT model for composite slab/two-dimensional geometry and compare it with other models for the

[1] Institut für Theoretische Physik, Lehrstuhl IV: Weltraum- und Astrophysik, Ruhr-Universität Bochum, D-44780 Bochum, Germany.
[2] Bartol Research Institute, and Department of Physics and Astronomy, University of Delaware, Newark, DE 19716.

dynamical correlation function. In § 3 we use QLT to calculate the pitch-angle Fokker-Planck coefficient and the parallel mean free path. In § 4 we use these results to calculate the perpendicular mean free path by applying NLGC theory. A comparison between the new theoretical results and observations is the subject of § 5, and the importance of nonlinear effects is discussed in § 6.

2. THE NONLINEAR ANISOTROPIC DYNAMCIAL TURBULENCE MODEL FOR COMPOSITE SLAB/TWO-DIMENSIONAL TURBULENCE

The key input into a cosmic-ray transport theory like QLT is the tensor P_{lm}, which describes the correlation of the turbulent magnetic fields:

$$P_{lm}(\boldsymbol{k}, t) = \langle \delta B_l(\boldsymbol{k}, t) \delta B_m^*(\boldsymbol{k}, 0) \rangle. \quad (1)$$

Therefore the $\boldsymbol{k}$-dependence and the time-dependence of the correlation tensor $P_{lm}(\boldsymbol{k}, t)$ have to be specified, which is done in §§ 2.1 and 2.2.

2.1. *Composite Slab/Two-Dimensional Turbulence Geometry*

For mathematical simplicity we employ the often used composite slab/two-dimensional model for the turbulence geometry (Bieber et al. 1994, 1996), which has been proposed as a realistic approximation for actual turbulence in the solar wind (Matthaeus et al. 1990; Bieber et al. 1996). In the composite model the correlation tensor is a superposition of a pure slab and a pure two-dimensional model. Therefore, we can write the total correlation tensor as

$$P_{lm}(\boldsymbol{k}, t) = P_{lm}^{0,\,\mathrm{slab}}(\boldsymbol{k}) \Gamma^{\mathrm{slab}}(k_\parallel, t) + P_{lm}^{0,\,2\mathrm{D}}(\boldsymbol{k}) \Gamma^{2\mathrm{D}}(k_\perp, t), \quad (2)$$

with the dynamical correlation functions $\Gamma^{\mathrm{slab}}(k_\parallel, t)$ and $\Gamma^{2\mathrm{D}}(k_\perp, t)$ and the time-independent correlation tensors $P_{lm}^{0,\,\mathrm{slab}}$ and $P_{lm}^{0,\,2\mathrm{D}}$. The tensors $P_{lm}^{0,\,i}$ are determined by the turbulence geometry and the wave spectrum, whereas the functions $\Gamma^i(\boldsymbol{k}, t)$ describe dynamical effects. In equation (2) we used the magnetostatic correlation tensor for the pure slab case,

$$P_{lm}^{0,\,\mathrm{slab}}(\boldsymbol{k}) = g^{\mathrm{slab}}(k_\parallel) \frac{\delta(k_\perp)}{k_\perp} \begin{cases} \delta_{lm} - \dfrac{k_l k_m}{k^2}, & l, m = x, y, \\ 0, & l \text{ or } m = z, \end{cases} \quad (3)$$

and the magnetostatic correlation tensor for the pure two-dimensional case,

$$P_{lm}^{0,\,2\mathrm{D}}(\boldsymbol{k}) = g^{2\mathrm{D}}(k_\perp) \frac{\delta(k_\parallel)}{k_\perp} \begin{cases} \delta_{lm} - \dfrac{k_l k_m}{k^2}, & l, m = x, y, \\ 0, & l \text{ or } m = z. \end{cases} \quad (4)$$

In equations (3) and (4) we assumed the case of vanishing magnetic helicity. The tensor for pure two-dimensional cases was defined in the same way as in Bieber et al. (1994, 1996). Such a two-dimensional model assumes that $\delta B_z = 0$, which is slightly different from the model that was used in Shalchi & Schlickeiser (2004b) where $\delta B_z \neq 0$. The functions g^{slab} and $g^{2\mathrm{D}}$ are the wave spectra for pure slab and pure two-dimensional geometry, respectively. For both we assume a power-law spectrum with energy, inertial, and dissipation range (see Fig. 1):

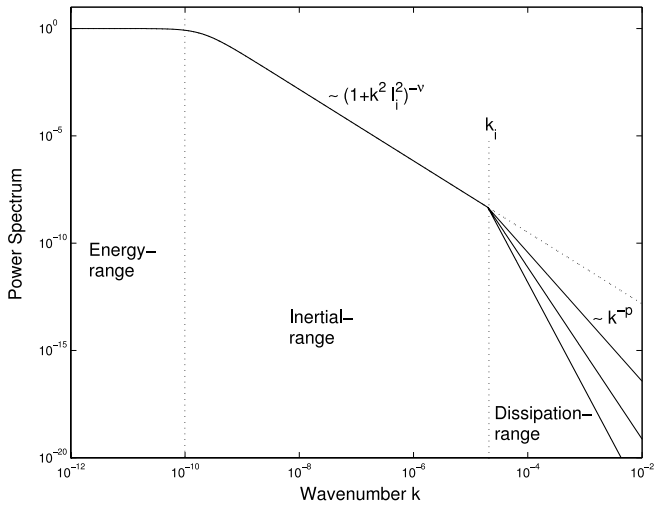

FIG. 1.—Power spectrum used for our calculations. We used a general spectrum with energy, inertial, and dissipation range. The dissipation wavenumber k_i (with i = slab, two-dimensional) divides the inertial range from the dissipation range.

$$g^{\mathrm{slab}}(k_\parallel) = \frac{C(\nu)}{2\pi} l_{\mathrm{slab}} \delta B_{\mathrm{slab}}^2 \begin{cases} (1 + k_\parallel^2 l_{\mathrm{slab}}^2)^{-\nu}, & k_\parallel \le k_{\mathrm{slab}}, \\ (1 + k_{\mathrm{slab}}^2 l_{\mathrm{slab}}^2)^{-\nu} (k_{\mathrm{slab}}/k_\parallel)^p, & k_\parallel \ge k_{\mathrm{slab}}, \end{cases} \quad (5)$$

$$g^{2\mathrm{D}}(k_\perp) = \frac{2C(\nu)}{\pi} l_{2\mathrm{D}} \delta B_{2\mathrm{D}}^2 \begin{cases} (1 + k_\perp^2 l_{2\mathrm{D}}^2)^{-\nu}, & k_\perp \le k_{2\mathrm{D}}, \\ (1 + k_{2\mathrm{D}}^2 l_{2\mathrm{D}}^2)^{-\nu} (k_{2\mathrm{D}}/k_\perp)^p, & k_\perp \ge k_{2\mathrm{D}}. \end{cases} \quad (6)$$

In both parts of the power spectrum we used the function $C(\nu) = (2\sqrt{\pi})^{-1} \Gamma(\nu)/\Gamma(\nu - 1/2)$.

Furthermore, we used the slab bendover scale l_{slab}; the two-dimensional bendover scale $l_{2\mathrm{D}}$; the slab dissipation wavenumber k_{slab}; the two-dimensional dissipation wavenumber $k_{2\mathrm{D}}$; the strength of the slab and the two-dimensional contribution to the turbulent fields, δB_{slab} and $\delta B_{2\mathrm{D}}$, respectively; the inertial range spectral index $s = 2\nu$; and the dissipation range spectral index p. In addition, the two dynamical correlation functions $\Gamma^{\mathrm{slab}}(k_\parallel, t)$ and $\Gamma^{2\mathrm{D}}(k_\perp, t)$ have to be determined, which is done below.

2.2. *The NADT Model for the Dynamical Correlation Functions*

In earlier treatments of dynamical turbulence, the decorrelation factors $\Gamma^i(\boldsymbol{k}, t)$ were established using simple approximations to the interactions responsible for temporal decorrelation of excitations near wavevector $\boldsymbol{k}$. In random sweeping and damping models, for example, a single parameter is introduced to estimate the rate of decorrelation at scale $1/k$, and this is assumed to be related to the large-scale Alfvén speed (see Table 1). In the plasma wave model the decorrelation rate is associated with oscillations at the Alfvén wave frequency. To improve these models, we note that in recent years there has been a more complete understanding of the timescales of MHD turbulence (e.g., Zhou et al. 2004) and the relation these may have to interactions between excitations that may be associated with either low-frequency or wavelike components of the turbulence spectrum (Matthaeus et al. 1990; Tu & Marsch 1993; Oughton et al. 2006). In the context of the two-component model, these ideas may

TABLE 1
Previous Models for the Dynamical Correlation Function

Model	$\Gamma(\boldsymbol{k}, t)$
Magnetostatic model	1
Damping model of dynamical turbulence	$e^{-\alpha v_A \lvert k \rvert t}$
Random sweeping model	$e^{-(\alpha v_A k t)^2}$
Plasma wave model for shear Alfvén waves	$e^{\pm i v_A k_\parallel t}$

Note.—Here v_A is the Alfvén velocity, and α is a parameter that allows one to adjust the strength of dynamical effects.

be used to determine reasonable approximations to the functions $\Gamma^{\rm slab}(k_\parallel, t)$ and $\Gamma^{\rm 2D}(k_\perp, t)$ that appear in equation (2).

These are to be interpreted as the time decorrelation rates of the fluctuations near the wavevector $\boldsymbol{k}$, normalized by the associated energy, and are related to the ordinary two-time (Eulerian) correlation function $E(t) = \langle \delta B_l(\boldsymbol{x}, t) \delta B_l^*(\boldsymbol{x}, 0) \rangle$ through $\int d^3k\, P_{ll}(\boldsymbol{k}, t) = E(t)$. Clearly $\Gamma(\boldsymbol{k}, 0) \equiv 1$, while $\lim_{t\to\infty} \Gamma(\boldsymbol{k}, t) = 0$. In various forms these dynamical decorrelation functions occupy a central role in analytical turbulence closures (see, e.g., Zhou et al. 2004).

In establishing timescales for MHD turbulence a crucial distinction is between those fluctuations having more wavelike dynamics and those having more hydrodynamic or "zero frequency" dynamics. For fluctuations that are predominantly incompressible (such as the solar wind), this characterization requires comparing estimates of the wave period with estimates of the nonlinear timescale, or eddy turnover time. When the wave timescale is the shorter of the two, wave effects are significant even when there is turbulence. If the nonlinear timescale is shorter, the nonlinear effects should dominate, and the wave effects are expected to be weaker.

In a practical sense, in which the spectrum is not made up of pure symmetry components, one would group with the slab population those wavevectors for which decorrelation occurs due to wave propagation, assumed here to be Alfvénic in character. This leads to a factor in $\Gamma^{\rm slab}$ of an oscillatory nature, with the angular frequency given by $\omega = \pm v_A k_\parallel$. In addition, the slablike component experiences resonant nonlinear triad interactions with the low-frequency two-dimensional component, as discussed by Shebalin et al. (1983) and Oughton et al. (1994). These interactions are characterized by a nonlinear time computed from the two-dimensional turbulence, without further wave influence (due to the resonance). For simplicity, we can estimate this influence by the *global* two-dimensional nonlinear timescale, $\tau_{nl}^{\rm 2D} = \alpha^{-1} l_{\rm 2D}/Z$, where Z is the two-dimensional turbulence amplitude (Oughton et al. 2006), α is a constant of order 1 related to the Karman-Taylor constants associated with the decay of the turbulence, and $l_{\rm 2D}$ is the spectral bendover scale of the two-dimensional component.

For the two-dimensional component, one reasonably groups together all the fluctuations for which the wavelike propagation effects are weak. Therefore, in constructing $\Gamma^{\rm 2D}$, no oscillatory factor need appear. For $k_\perp$ sufficiently small, the two-dimensional fluctuations lie in the non-self-similar energy-containing range, and the estimate for the decorrelation rate is again the global rate $1/\tau_{nl}^{\rm 2D}$. For smaller two-dimensional fluctuations the decorrelation can be estimated using a steady inertial range $k_\perp^{-5/3}$ approximation, which is essentially what enters the steady Goldreich & Sridhar (1995) spectral theory. In this case the nonlinear timescale $\tau_{nl}^{\rm 2D}(k_\perp) = 1/(k_\perp u_{k_\perp})$, where the turbulence amplitude $u_{k_\perp} = [k_\perp E(k_\perp)]^{1/2}$ for two-dimensional steady inertial range wavenumber spectrum $E(k_\perp) \sim k_\perp^{-5/3}$. This timescale is shorter than that of the energy-containing range and varies with $k_\perp$ according to $\tau_{nl}^{\rm 2D}(k_\perp) = \tau_{nl}^{\rm 2D}/(k_\perp l_{\rm 2D})^{2/3}$.

Assembling these results, we obtain a new, more realistic model for $\Gamma^{\rm slab}$ and $\Gamma^{\rm 2D}$, which we call the nonlinear anisotropic dynamical turbulence (NADT) model. For the function $\Gamma^{\rm slab}(k_\perp, t)$ we have

$$\Gamma^{\rm slab}(k_\parallel, t) = e^{-\gamma^{\rm slab} t} e^{i\omega t}, \tag{7}$$

with

$$\gamma^{\rm slab} = (\tau_{nl}^{\rm 2D})^{-1} = \beta = \alpha \frac{Z}{l_{\rm 2D}}, \tag{8}$$

and with the plasma wave dispersion relation of shear Alfvén waves,

$$\omega = j v_A k_\parallel. \tag{9}$$

The parameter j is used to track the wave direction ($j = +1$ is used for forward and $j = -1$ for backward to the ambient magnetic field–propagating Alfvén waves). A lot of studies have addressed the direction of propagation of Alfvénic turbulence; see, for instance, Bavassano (2003). In general one would expect that closer to the Sun, most waves should propagate forward, and far away from the Sun, the wave intensities should be equal for both directions. In the current paper we are interested in turbulence parameters at 1 AU. Thus, we simply assume that all waves propagate forward, and we therefore set $j = +1$.

For the function $\Gamma^{\rm 2D}(\boldsymbol{k}, t)$ we have

$$\Gamma^{\rm 2D}(k_\perp, t) = e^{-\gamma^{\rm 2D} t}, \tag{10}$$

with

$$\gamma^{\rm 2D} = \beta \begin{cases} 1, & k_\perp l_{\rm 2D} \le 1, \\ (k_\perp l_{\rm 2D})^{2/3}, & k_\perp l_{\rm 2D} \ge 1. \end{cases} \tag{11}$$

The parameter Z in equation (8) can be expressed by the strength of the two-dimensional component $\delta B_{\rm 2D}/B_0$ and the Alfvén speed v_A:

$$Z = \sqrt{2} \frac{\delta B_{\rm 2D}}{\sqrt{4\pi\rho_d}} = \sqrt{2} v_A \frac{\delta B_{\rm 2D}}{B_0}, \tag{12}$$

and we find

$$\beta = \sqrt{2}\alpha \frac{v_A}{l_{\rm 2D}} \frac{\delta B_{\rm 2D}}{B_0}. \tag{13}$$

The model defined above takes into account the plasma wave character of the turbulence. In order to determine the transport coefficients of the isotropic part of the particle distribution function, as the parallel mean free path, we must restrict our calculations to $\epsilon = v_A/v \ll 1$ (Schlickeiser 2002). In turn we employ the NADT model to determine the parallel mean free path within the quasi-linear approach. Transport perpendicular to the background field is considered in § 4.

3. THE QUASI-LINEAR PARALLEL MEAN FREE PATH

In the current paper we employ QLT to calculate the parallel mean free path. QLT can be seen as a first-order perturbation theory in the small parameter $\delta B/B_0$. Whereas it was shown previously (e.g., Michalek & Ostrowski 1996) that QLT is accurate, even if $\delta B \approx B_0$, if we assume slab geometry and a wave spectrum without dissipation range, it was realized by more recent test particle simulations that for nonslab models and for steep

wave spectra, nonlinear effects are important and QLT is no longer accurate. In this section we simply assume the validity of QLT for the turbulence model considered in the current paper, but we refer to § 6 where nonlinear effects in cosmic-ray transport theory are discussed.

According to Jokipii (1966), Hasselmann & Wibberenz (1968), Earl (1974), and Shalchi (2006), the parallel mean free path results from the pitch-angle cosine average of the inverse pitch-angle Fokker-Planck coefficient $D_{\mu\mu}$ as

$$\lambda_{\parallel} = \frac{3v}{8}\int_{-1}^{+1} d\mu\, \frac{(1-\mu^2)^2}{D_{\mu\mu}(\mu)}. \tag{14}$$

Within the composite model the total Fokker-Planck coefficient can be written as a superposition of the pitch-angle Fokker-Planck coefficient for pure slab and pure two-dimensional geometry,

$$D_{\mu\mu}^{\rm total}(\mu) = D_{\mu\mu}^{\rm slab}(\mu) + D_{\mu\mu}^{\rm 2D}(\mu). \tag{15}$$

Therefore, we must calculate both contributions. According to Teufel & Schlickeiser (2002, eq. [25]) the pitch-angle Fokker-Planck coefficient can be written as

$$\begin{aligned} D_{\mu\mu}^{i}(\mu) &= \frac{\Omega^2(1-\mu^2)}{2B_0^2} \\ &\times \int d^3k \sum_{n=-\infty}^{+\infty} \int d^3k \left\{ J_{n+1}^2\left(\frac{k_\perp v_\perp}{\Omega}\right) P_{RR}^{0,i}(\boldsymbol{k}) \right. \\ &+ J_{n-1}^2\left(\frac{k_\perp v_\perp}{\Omega}\right) P_{LL}^{0,i}(\boldsymbol{k}) - J_{n+1}\left(\frac{k_\perp v_\perp}{\Omega}\right) J_{n-1}\left(\frac{k_\perp v_\perp}{\Omega}\right) \\ &\times \left. \left[P_{RL}^{0,i}(\boldsymbol{k}) e^{+2i\Psi} + P_{LR}^{0,i}(\boldsymbol{k}) e^{-2i\Psi} \right] \right\} R_n^i(\boldsymbol{k}), \end{aligned} \tag{16}$$

if we use helical coordinates

$$\begin{aligned} \delta B_L &= \frac{1}{\sqrt{2}}\left(\delta B_x + i\delta B_y\right), \\ \delta B_R &= \frac{1}{\sqrt{2}}\left(\delta B_x - i\delta B_y\right), \end{aligned} \tag{17}$$

and if we neglect electric fields. In equation (16) we used the resonance function

$$R_n^i(\boldsymbol{k}) = {\rm Re}\left[\int_0^\infty dt\, e^{-i(k_\parallel v_\parallel + n\Omega)t} \Gamma^i(\boldsymbol{k}, t)\right]. \tag{18}$$

In turn we evaluate equation (16) for pure slab and pure two-dimensional geometry.

3.1. *The Pitch-Angle Fokker-Planck Coefficient for Pure Slab Geometry*

For pure slab geometry we have, according to Teufel & Schlickeiser (2002, eq. [33]),

$$\begin{aligned} P_{RR}^0 &= P_{LL}^0 = g^{\rm slab}\left(k_\parallel\right)\frac{\delta(k_\perp)}{k_\perp}, \\ P_{RL}^0 &= P_{LR}^0 = 0, \end{aligned} \tag{19}$$

if we assume vanishing magnetic helicity. For the pitch-angle Fokker-Planck coefficient we then find

$$D_{\mu\mu}^{\rm slab} = \frac{\pi\Omega^2(1-\mu^2)}{B_0^2}\int_{-\infty}^{+\infty} dk_\parallel\, g^{\rm slab}\left(k_\parallel\right) \sum_{n=\pm 1} R_n^{\rm slab}\left(k_\parallel\right). \tag{20}$$

The resonance function for pure slab has the form

$$R_n^{\rm slab}\left(k_\parallel\right) = {\rm Re}\left[\int_0^\infty dt\, e^{-i(k_\parallel v_\parallel + n\Omega)t}\Gamma^{\rm slab}\left(k_\parallel, t\right)\right]. \tag{21}$$

With $\Gamma^{\rm slab}(k_\parallel, t) = e^{-\beta t} e^{iv_{\rm A}k_\parallel t}$, the integral in equation (21) is elementary, and we obtain

$$R_n^{\rm slab} = \frac{\beta}{\beta^2 + \left(k_\parallel v_\parallel + n\Omega - v_{\rm A}k_\parallel\right)^2}. \tag{22}$$

With this Breit-Wigner-type resonance function, the slab Fokker-Planck coefficient can be written as

$$D_{\mu\mu}^{\rm slab} = \frac{2\pi\Omega^2(1-\mu^2)}{B_0^2}\int_0^\infty dk_\parallel g^{\rm slab}(k_\parallel)\sum_{n=\pm 1}\frac{\beta}{\beta^2 + \left(k_\parallel v_\parallel + n\Omega - v_{\rm A}k_\parallel\right)^2}. \tag{23}$$

With the integral transformation $x = l_{\rm slab}k_\parallel$ and with the parameters $R = R_L/l_{\rm slab} = v/(\Omega l_{\rm slab})$ and $\epsilon = v_{\rm A}/v$, we obtain

$$\begin{aligned} D_{\mu\mu}^{\rm slab} &= \frac{2\pi(1-\mu^2)}{B_0^2 l_{\rm slab}} \\ &\times \int_0^\infty dx\, g^{\rm slab}\left(k_\parallel = \frac{x}{l_{\rm slab}}\right)\sum_{n=\pm 1}\frac{\beta}{(\beta/\Omega)^2 + \left[xR(\mu-\epsilon)+n\right]^2}. \end{aligned} \tag{24}$$

The slab spectrum of equation (5) can be written as

$$g^{\rm slab}(x) = \frac{C(\nu)}{2\pi} l_{\rm slab}\delta B_{\rm slab}^2 h^{\rm slab}(x), \tag{25}$$

with

$$h^{\rm slab}(x) = \begin{cases} (1+x^2)^{-\nu}, & x \le \xi_{\rm slab}, \\ \left(1+\xi_{\rm slab}^2\right)^{-\nu}\left(\dfrac{\xi_{\rm slab}}{x}\right)^p, & x \ge \xi_{\rm slab}, \end{cases} \tag{26}$$

where we used $\xi_{\rm slab} = l_{\rm slab}k_{\rm slab}$. Then we find for the dimensionless Fokker-Planck coefficient $\tilde{D}_{\mu\mu}^{\rm slab} = (l_{\rm slab}/v)D_{\mu\mu}^{\rm slab}$,

$$\begin{aligned} \tilde{D}_{\mu\mu}^{\rm slab} &= \frac{C(\nu)(1-\mu^2)}{R}\frac{\delta B_{\rm slab}^2}{B_0^2} \\ &\times \int_0^\infty dx\, h^{\rm slab}(x)\sum_{n=\pm 1}\frac{\beta/\Omega}{(\beta/\Omega)^2 + \left[xR(\mu-\epsilon)+n\right]^2}. \end{aligned} \tag{27}$$

The parameter β/Ω can be expressed by

$$\beta/\Omega = \sqrt{2}\alpha\epsilon\rho\frac{\delta B_{\rm 2D}}{B_0}R \equiv \sqrt{2}\alpha\frac{v_{\rm A}}{v}\frac{R_L}{l_{\rm 2D}}\frac{\delta B_{\rm 2D}}{B_0}, \tag{28}$$

where we used $\rho = l_{\rm slab}/l_{\rm 2D}$. A numerical investigation of the integral of equation (27) is time-consuming, and therefore we present analytical approximations of equation (27) in the Appendix.

3.2. *The Pitch-Angle Fokker-Planck Coefficient for Pure Two-Dimensional Geometry*

According to Shalchi & Schlickeiser (2004b, eq. [13]), we have for pure two-dimensional geometry,

$$P_{LL}^0 = P_{RR}^0 = \frac{1}{2} g(k_\perp) \frac{\delta(k_\parallel)}{k_\perp},$$
$$P_{RL}^0 = -\frac{1}{2} g(k_\perp) \frac{\delta(k_\parallel)}{k_\perp} e^{-2i\Psi},$$
$$P_{LR}^0 = -\frac{1}{2} g(k_\perp) \frac{\delta(k_\parallel)}{k_\perp} e^{+2i\Psi}; \quad (29)$$

with equation (16) we obtain for the two-dimensional pitch-angle Fokker-Planck coefficient,

$$D_{\mu\mu}^{\rm 2D} = \frac{2\pi\Omega^2(1-\mu^2)}{B_0^2} \int_0^\infty dk_\perp\, g^{\rm 2D}(k_\perp) \sum_{n=-\infty}^{+\infty} R_n^{\rm 2D}(k_\perp) \frac{n^2 J_n^2(W)}{W^2}, \quad (30)$$

with

$$W = \frac{k_\perp v}{\Omega} \sqrt{1-\mu^2} = k_\perp R_L \sqrt{1-\mu^2} \quad (31)$$

and the resonance function

$$R_n^{\rm 2D} = {\rm Re}\left[\int_0^\infty dt\, e^{-in\Omega t} \Gamma^{\rm 2D}(k_\perp, t) \right]. \quad (32)$$

With $\Gamma^{\rm 2D}(k_\perp, t) = e^{-\gamma^{\rm 2D} t}$, the resonance function can be rewritten as

$$R_n^{\rm 2D} = {\rm Re}\left(\int_0^\infty dt\, e^{-in\Omega t - \gamma^{\rm 2D} t} \right) = \frac{\gamma^{\rm 2D}}{(\gamma^{\rm 2D})^2 + (n\Omega)^2}, \quad (33)$$

and we obtain for the pitch-angle Fokker-Planck coefficient

$$D_{\mu\mu}^{\rm 2D} = \frac{2\pi\Omega^2(1-\mu^2)}{B_0^2} \times \int_0^\infty dk_\perp\, g^{\rm 2D}(k_\perp) \sum_{n=-\infty}^{+\infty} \frac{\gamma^{\rm 2D}}{(\gamma^{\rm 2D})^2 + (n\Omega)^2} \frac{n^2 J_n^2(W)}{W^2}. \quad (34)$$

With the approximation of Shalchi & Schlickeiser (2004b, eq. [19]),

$$\sum_{n=1}^\infty \frac{n^2}{n^2+y^2} J_n^2(x) \approx \frac{x^2}{2} \frac{1}{x^2+2y^2+2}, \quad (35)$$

$D_{\mu\mu}^{\rm 2D}$ can be simplified to

$$D_{\mu\mu}^{\rm 2D} = \frac{2\pi(1-\mu^2)}{B_0^2} \int_0^\infty dk_\perp\, g^{\rm 2D}(k_\perp) \frac{\gamma^{\rm 2D}}{W^2 + 2(\gamma^{\rm 2D}/\Omega)^2 + 2}. \quad (36)$$

Using the integral transformation $x = k_\perp l_{\rm 2D}$ and $\rho = l_{\rm slab}/l_{\rm 2D}$, we obtain

$$D_{\mu\mu}^{\rm 2D} = \frac{2\pi(1-\mu^2)}{B_0^2 l_{\rm 2D}} \int_0^\infty dx\, g^{\rm 2D}\left(k_\perp = \frac{x}{l_{\rm 2D}}\right) \times \frac{\gamma^{\rm 2D}}{\left(xR\rho\sqrt{1-\mu^2}\right)^2 + 2(\gamma^{\rm 2D}/\Omega)^2 + 2}. \quad (37)$$

The two-dimensional spectrum of equation (6) can be written as

$$g^{\rm 2D} = \frac{2C(\nu)}{\pi} l_{\rm 2D} \delta B_{\rm 2D}^2 h^{\rm 2D}(x), \quad (38)$$

with

$$h^{\rm 2D}(x) = \begin{cases} (1+x^2)^{-\nu}, & x \le \xi_{\rm 2D}, \\ \left(1+\xi_{\rm 2D}^2\right)^{-\nu} \left(\dfrac{\xi_{\rm 2D}}{x}\right)^p, & x \ge \xi_{\rm 2D}, \end{cases} \quad (39)$$

where we used $\xi_{\rm 2D} = l_{\rm 2D} k_{\rm 2D}$. Then we find for the dimensionless Fokker-Planck coefficient $\tilde{D}_{\mu\mu}^{\rm 2D} = (l_{\rm slab}/v) D_{\mu\mu}^{\rm 2D}$,

$$\tilde{D}_{\mu\mu}^{\rm 2D} = \frac{4C(\nu)(1-\mu^2)}{R} \frac{\delta B_{\rm 2D}^2}{B_0^2} \times \int_0^\infty dx\, h^{\rm 2D}(x) \frac{\tilde{\gamma}^{\rm 2D}}{\left(xR\rho\sqrt{1-\mu^2}\right)^2 + 2(\tilde{\gamma}^{\rm 2D})^2 + 2}, \quad (40)$$

with

$$\tilde{\gamma}^{\rm 2D} = \frac{\gamma^{\rm 2D}}{\Omega} = \frac{\beta}{\Omega} \begin{cases} 1, & x \le 1, \\ x^{2/3}, & x \ge 1. \end{cases} \quad (41)$$

The integrals can be solved numerically. Together with the slab results of § 3.1, we can determine the total Fokker-Planck coefficient in a composite slab/two-dimensional geometry. If we express the parallel mean free path by the dimensionless pitch-angle Fokker-Planck coefficients, we find for composite geometry,

$$\lambda_\parallel = \frac{3}{4} l_{\rm slab} \int_0^1 d\mu\, \frac{(1-\mu^2)^2}{\tilde{D}_{\mu\mu}^{\rm slab}(\mu) + \tilde{D}_{\mu\mu}^{\rm 2D}(\mu)}. \quad (42)$$

To replace $\tilde{D}_{\mu\mu}^{\rm slab}$ and $\tilde{D}_{\mu\mu}^{\rm 2D}$, we can use equations (27) and (40). Together with the analytical approximations for $\tilde{D}_{\mu\mu}^{\rm slab}$ presented in the Appendix, it is straightforward to calculate the parallel mean free path numerically, which is done in § 5.

4. THE NONLINEAR PERPENDICULAR MEAN FREE PATH

In § 3 we only considered parallel spatial diffusion, but particle propagation in the direction perpendicular to the background field is not less important. Here we employ the recently proposed NLGC theory (Matthaeus et al. 2003) to compute the perpendicular mean free path. In NLGC theory the parallel mean free path is simply an input parameter into an integral equation that determines the perpendicular mean free path. According to Shalchi et al. (2004a) this integral equation can be written as

$$\kappa_\perp = \frac{a^2 v^2}{3B_0^2} \left\{ \int d^3k\, P_{xx}^{0,{\rm slab}}(\boldsymbol{k}) \times \int_0^\infty dt\, e^{-vt/\lambda_\parallel - k_\perp^2 \kappa_\perp t - k_\parallel^2 \kappa_\parallel t} {\rm Re}\left[\Gamma^{\rm slab}(k_\parallel, t)\right] + \int d^3k\, P_{xx}^{0,{\rm 2D}}(\boldsymbol{k}) \times \int_0^\infty dt\, e^{-vt/\lambda_\parallel - k_\perp^2 \kappa_\perp t - k_\parallel^2 \kappa_\parallel t} {\rm Re}\left[\Gamma^{\rm 2D}(k_\perp, t)\right] \right\}. \quad (43)$$

Applying equations (7) and (10),

$$\mathrm{Re}\left[\Gamma^{\mathrm{slab}}\left(k_{\parallel},t\right)\right]=\cos\left(\omega t\right)e^{-\gamma^{\mathrm{slab}}t},$$
$$\mathrm{Re}\left[\Gamma^{\mathrm{2D}}(k_{\perp},t)\right]=e^{-\gamma^{\mathrm{2D}}t}, \tag{44}$$

and using

$$\int_0^{\infty}dt\,e^{-\nu t/\lambda_{\parallel}-k_{\perp}^2\kappa_{\perp}t-k_{\parallel}^2\kappa_{\parallel}t}\cos\left(\omega t\right)e^{-\gamma t}$$
$$=\frac{\nu/\lambda_{\parallel}+k_{\perp}^2\kappa_{\perp}+k_{\parallel}^2\kappa_{\parallel}+\gamma}{\left(\nu/\lambda_{\parallel}+k_{\perp}^2\kappa_{\perp}+k_{\parallel}^2\kappa_{\parallel}+\gamma\right)^2+\omega^2}, \tag{45}$$

we obtain

$$\kappa_{\perp}=\frac{a^2v^2}{3B_0^2}\left[\int d^3k\,P_{xx}^{0,\,\mathrm{slab}}(\boldsymbol{k})\frac{\nu/\lambda_{\parallel}+k_{\perp}^2\kappa_{\perp}+k_{\parallel}^2\kappa_{\parallel}+\gamma^{\mathrm{slab}}}{\left(\nu/\lambda_{\parallel}+k_{\perp}^2\kappa_{\perp}+k_{\parallel}^2\kappa_{\parallel}+\gamma^{\mathrm{slab}}\right)^2+\omega^2}\right.$$
$$\left.+\int d^3k\,P_{xx}^{0,\,\mathrm{2D}}(\boldsymbol{k})\frac{1}{\nu/\lambda_{\parallel}+k_{\perp}^2\kappa_{\perp}+k_{\parallel}^2\kappa_{\parallel}+\gamma^{\mathrm{2D}}}\right]. \tag{46}$$

With equations (3) and (4) for $P_{xx}^{0,\,\mathrm{slab}}$ and $P_{xx}^{0,\,\mathrm{2D}}$, with both the wave spectra of equations (25) and (38), and by applying $\lambda_{\parallel}=(3/\nu)\kappa_{\parallel}$ and $\lambda_{\perp}=(3/\nu)\kappa_{\perp}$, we finally find

$$\frac{\lambda_{\perp}}{\lambda_{\parallel}}=2a^2C(\nu)\left(\frac{\delta B_{\mathrm{slab}}^2}{B_0^2}\int_0^{\infty}dx\right.$$
$$\times h^{\mathrm{slab}}(x)\frac{1+\left[\lambda_{\parallel}^2/\left(3l_{\mathrm{slab}}^2\right)\right]x^2+\left(\lambda_{\parallel}/\nu\right)\gamma^{\mathrm{slab}}}{\left\{1+\left[\lambda_{\parallel}^2/\left(3l_{\mathrm{slab}}^2\right)\right]x^2+\left(\lambda_{\parallel}/\nu\right)\gamma^{\mathrm{slab}}\right\}^2+\left[\left(\epsilon\lambda_{\parallel}/l_{\mathrm{slab}}\right)x\right]^2}$$
$$\left.+\frac{\delta B_{\mathrm{2D}}^2}{B_0^2}\int_0^{\infty}dx\,h^{\mathrm{2D}}(x)\frac{1}{1+\left[\lambda_{\parallel}\lambda_{\perp}/\left(3l_{\mathrm{2D}}^2\right)\right]x^2+\left(\lambda_{\parallel}/\nu\right)\gamma^{\mathrm{2D}}}\right). \tag{47}$$

To replace γ^{slab} and γ^{2D}, we can use

$$\frac{\lambda_{\parallel}}{\nu}\gamma^{\mathrm{slab}}=\frac{\lambda_{\parallel}}{Rl_{\mathrm{slab}}}\frac{\beta}{\Omega} \tag{48}$$

and

$$\frac{\lambda_{\parallel}}{\nu}\gamma^{\mathrm{2D}}=\frac{\lambda_{\parallel}}{Rl_{\mathrm{slab}}}\frac{\beta}{\Omega}\begin{cases}1, & x\le 1,\\ x^{2/3}, & x\ge 1.\end{cases} \tag{49}$$

The parameter β is defined in equation (13), and for a^2 we assume $a^2=\frac{1}{3}$. This choice of the parameter a^2 was suggested by Matthaeus et al. (2003) to achieve agreement between NLGC theory and test particle simulations in magnetostatic turbulence. A theoretical justification of $a^2=\frac{1}{3}$ has not been given so far. A numerical investigation of equation (47) is straightforward, and the results are presented together with the QLT results for parallel diffusion in § 5.

5. NUMERICAL RESULTS WITHIN THE NADT MODEL

In this section we evaluate the formulas for the mean free paths derived in §§ 3 and 4 numerically for the parameter set of Table 2, which should be appropriate for interplanetary conditions at 1 AU.

TABLE 2

Parameters Used for our Numerical Calculations

Parameter	Symbol	Value
Inertial range spectral index	2ν	5/3
Dissipation range spectral index	p	3
Alfvén speed	v_{A}	33.5 km s^{-1}
Slab bendover scale	l_{slab}	0.030 AU
2D bendover scale	l_{2D}	$0.1l_{\mathrm{slab}}$
Slab dissipation wavenumber	k_{slab}	3×10^6 AU^{-1}
2D dissipation wavenumber	k_{2D}	3×10^6 AU^{-1}
Mean field	B_0	4.12 nT
Turbulence strength	$\delta B/B_0$	1
Slab fraction	$\delta B_{\mathrm{slab}}^2$	$0.2\delta B^2$
2D fraction	δB_{2D}^2	$0.8\delta B^2$

Notes.—The values should be appropriate for heliospheric parameters at 1 AU. If a parameter is different from the values below, we note this separately in the corresponding figures and discussions.

All formulas are dependent on the parameter ϵ, which can be expressed as

$$\epsilon=\frac{v_{\mathrm{A}}}{v}=\frac{v_{\mathrm{A}}}{c}\frac{\sqrt{R_0^2+R^2}}{R}, \tag{50}$$

with

$$R_0=\frac{1}{l_{\mathrm{slab}}B_0}\begin{cases}0.511\ \mathrm{MV}, & \text{for } e^-,\\ 938\ \mathrm{MV}, & \text{for } p^+.\end{cases} \tag{51}$$

For the heliospheric parameters considered in the current paper, we have for electrons $R_0(e^-)\approx 9.2\times10^{-5}$ and protons $R_0(p^+)\approx 0.169$. Because we must take into account the restriction $\epsilon=v_{\mathrm{A}}/v\ll 1$ (see end of § 2.2), we can only consider rigidities that satisfy the following condition:

$$R\gg\frac{R_0}{\sqrt{(c/v_{\mathrm{A}})^2-1}}\approx R_0\frac{v_{\mathrm{A}}}{c}. \tag{52}$$

For $v_{\mathrm{A}}=33.5$ km s^{-1}, we find for electrons the restriction $R(e^-)\gg10^{-8}$ and for protons $R(p^+)\gg2\times10^{-5}$. Therefore, the proton results presented in the current paper could be invalid for $R(p^+)\le2\times10^{-5}$.

In turn we compare NADT results with observations and with other turbulence models. Furthermore, we discuss the dependence of $\lambda_{\parallel}$ and $\lambda_{\perp}$ on different turbulence parameters.

5.1. *Pitch-Angle Diffusion within the NADT Model*

Figure 2 shows the pitch-angle Fokker-Planck coefficients calculated within the NADT model. In general the pitch-angle Fokker-Planck coefficient is no longer equal to zero at 90° ($\mu=0$) as in the magnetostatic model, so that we no longer obtain an infinitely large, parallel mean free path as in magnetostatic models. It should be noted, however, that QLT itself is questionable close to 90°. By considering Figure 2 we find that, at least for protons, pitch-angle scattering close to 90° is very strong due to the dynamical effects. Therefore, one could assume that nonlinear effects that also lead to nonvanishing pitch-angle scattering at 90° could be neglected (see discussions is § 6.1).

5.2. *Parallel and Perpendicular Diffusion in Comparison with Observations*

Here we present theoretical results for the parallel and perpendicular mean free paths obtained within the NADT model. We

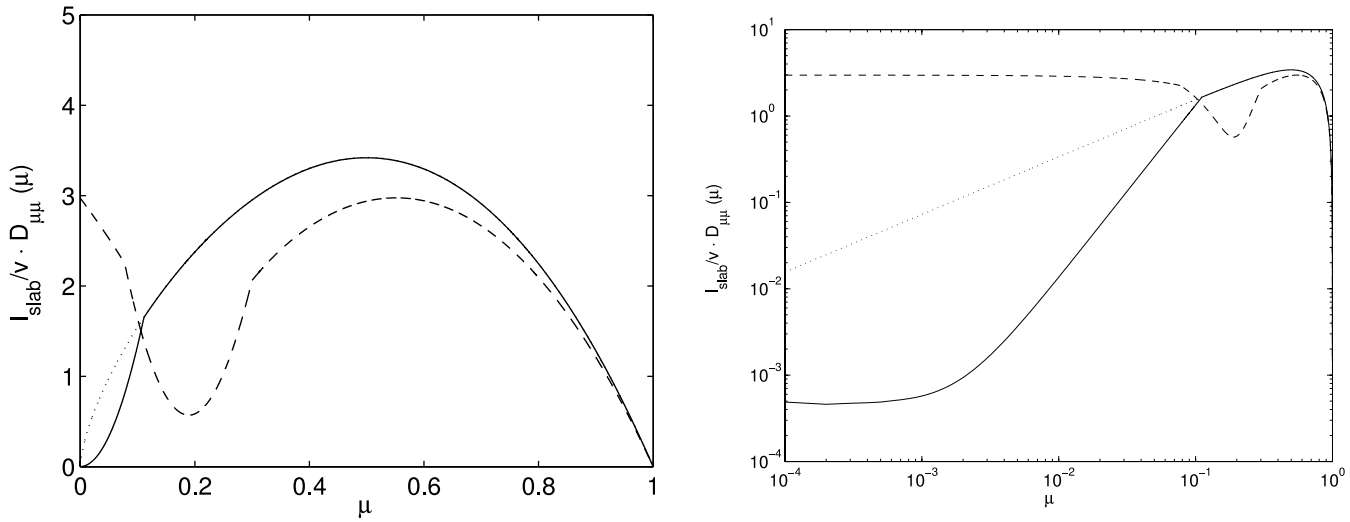

FIG. 2.—Pitch-angle Fokker-Planck coefficient calculated within the NADT model for protons (*dashed line*) and electrons (*solid line*). The magnetostatic dissipationless model is also shown (*dotted line*). The left panel shows a linear and the right panel a logarithmic plot of the dimensionless pitch-angle Fokker-Planck coefficient $\tilde{D}_{\mu\mu}$ as a function of the pitch-angle cosine μ. All results are for a nearly pure slab geometry ($\delta B^2_{slab}/B^2_0 = 0.9$) and for small rigidities, $R = 10^{-4}$.

compare our new results with the Palmer consensus (Palmer 1982), Jovian electrons (Chenette et al. 1977), *Ulysses* measurements of Galactic protons (Burger et al. 2000), and pickup ion observations (Gloeckler et al. 1995, Möbius et al. 1998).

5.2.1. *Parallel Mean Free Paths in Comparison with the Palmer Consensus and Pickup Ion Observations*

In Figure 3 we show the parallel mean free path in comparison with observations. Our results are not much different from results obtained within the DT model (damping model of dynamical turbulence, Bieber et al. 1994), but here the two-dimensional contribution to the Fokker-Planck coefficient plays a crucial role (see §§ 5.4 and 5.6). Palmer (1982) concluded that the parallel mean free path for rigidities between 0.5 and 5000 MV is 0.08 AU $\leq \lambda_{\parallel} \leq$ 0.3 AU (but see also Reames 1999). According to Figure 3, our new theoretical results agree very well with the Palmer consensus range.

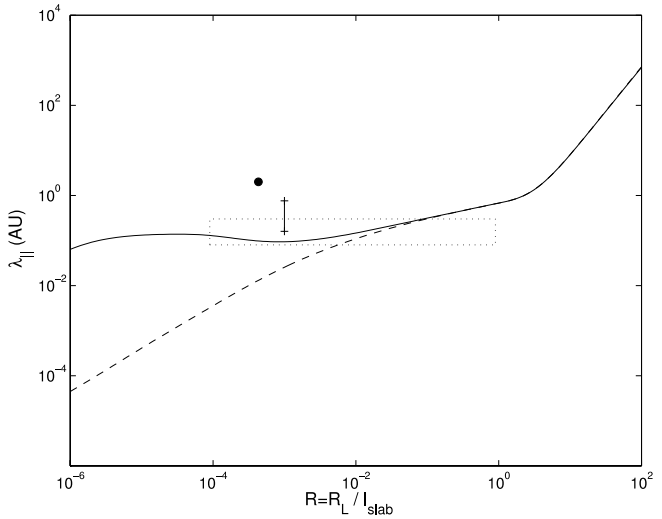

FIG. 3.—Parallel mean free path $\lambda_{\parallel}$. Shown are QLT results for electrons (*solid line*) and protons (*dashed line*) in comparison with different observations: Palmer consensus (Palmer 1982, *box*), *Ulysses* observations (Gloeckler et al. 1995, *circle*), and AMPTE spacecraft observations (Möbius et al. 1998, *vertical line*).

In addition to the Palmer results we compare our results also with pickup ion observations:

1. Gloeckler et al. (1995) concluded from *Ulysses* observations that the parallel mean free paths of pickup protons is 2 AU at 2.4 MV rigidity (they stated conservatively that $\lambda_{\parallel}$ is of order 1 AU, but actually they obtained the best fit for 2 AU). It should be noted that this observation was at high heliographic latitudes and at a heliocentric distance of 2.34 AU; these differences should be remembered when comparing with observations at Earth orbit.

2. Möbius et al. (1998) concluded from Active Magnetospheric Particle Tracer Explorers (AMPTE) spacecraft observations that the parallel mean free paths of pickup helium ranges from 0.16 to 0.76 AU at 5.6 MV rigidity in the data they analyzed.

Both results are also shown in Figure 3. The Möbius et al. (1998) observations are close to our theoretical results, but the Gloeckler et al. (1995) measurements are much larger than our theoretical predictions. We expect that the reason for this discrepancy is that the Gloeckler et al. (1995) observation was at high heliographic latitudes and at a heliocentric distance of 2.34 AU. For such conditions the turbulence parameters are expected to be quite different from the values we used for our theoretical calculations (see Table 2). For example, if we would decrease the strength of turbulence $\delta B/B_0$, we would obtain a much larger parallel mean free path. Therefore, we expect that the Gloeckler et al. (1995) and the Möbius et al. (1998) observations can be reproduced by changing the turbulence parameters.

5.2.2. *Perpendicular Mean Free Paths in Comparison with Jovian Electrons and Galactic Protons*

In Figure 4 we show perpendicular mean free paths at 1 AU calculated with NLGC theory within the NADT model compared with observations. Our new results agree very well with observational determinations from Jovian electrons (Chenette et al. 1977) and *Ulysses* measurements of Galactic protons (Burger et al. 2000). Palmer (1982) concluded that an average perpendicular diffusion coefficient at 1 AU of $\kappa_{\perp} c/v \approx 10^{21}$ cm^2 s^{-1} and therefore $\lambda_{\perp} \approx 0.0067$ AU. In this paper the author pointed out that the spread around this average was rather large. Thus, the Palmer result for $\lambda_{\perp}$ agrees with our new theoretical results.

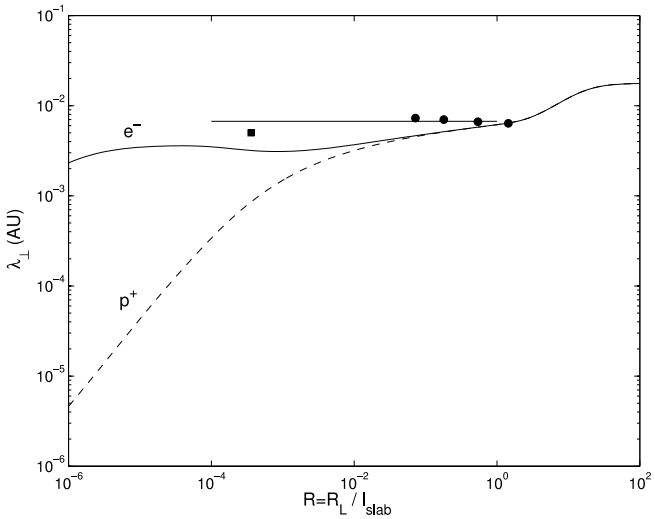

FIG. 4.—Perpendicular mean free path $\lambda_\perp$. Shown are results for electrons (*solid line*) and protons (*dashed line*) in comparison with Jovian electrons (Chenette et al. 1977, *square*), *Ulysses* measurements of Galactic protons (Burger et al. 2000, *circles*), and the Palmer (1982, *horizontal line*) value.

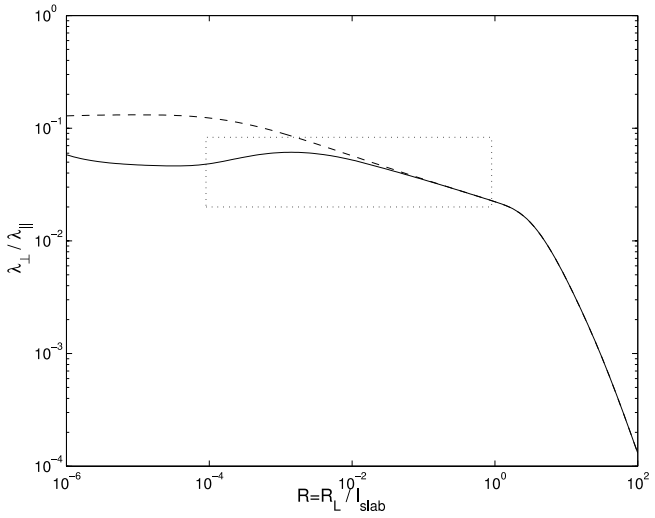

FIG. 5.—Ratio $\lambda_\perp/\lambda_\parallel$. Shown are QLT results for electrons (*solid line*) and protons (*dashed line*) in comparison with observations (Palmer 1982, *box*).

5.2.3. *The Ratio $\lambda_\perp/\lambda_\parallel$ in Comparison with the Palmer Consensus*

In addition, the ratio $\lambda_\perp/\lambda_\parallel$ can be compared with observations of Palmer (1982). By combining the average values for $\lambda_\perp$ (see § 4) with the Palmer consensus values for $\lambda_\parallel$, we find that $0.02 \leq \lambda_\perp/\lambda_\parallel \leq 0.083$. As shown by Figure 5, the theoretical results of the present paper agree very well with the Palmer consensus. QLT was not applied for perpendicular transport within the NADT model, but from Shalchi & Schlickeiser (2004a) we expect a rather large value ($\lambda_\perp/\lambda_\parallel \sim 10^3$), which does not agree with observations. This is one reason why we conclude that QLT is not appropriate for describing perpendicular transport (see further comments in § 6.3).

5.3. *The Influence of the Plasma Wave Dispersion Relation*

In general NADT results are different from magnetostatic results because of two reasons:

1. The dynamical effects described by the exponential functions $e^{-\gamma^{\rm slab}t}$ and $e^{-\gamma^{\rm 2D}t}$ in the dynamical correlation functions cause resonance broadening. Such resonance broadening effects have a strong influence on the Fokker-Planck and spatial diffusion coefficients, at least for pitch angles close to 90°.
2. The plasma wave dispersion relation, which only enters the slab dynamical correlation function by the factor $e^{i\omega t}$, causes a shift in the resonance condition.

All calculations presented in this paper were done with both effects, but we repeated all calculations by setting $\omega = 0$. By comparing results with and without the plasma wave dispersion relation ω, we noted a coincidence between all mean free paths except for the proton results of Figure 9 where we find a slight influence of ω (see comments in § 5.6). Therefore, we come to the conclusion that within the NADT model plasma wave effects can be neglected for most parameter regimes.

5.4. *Influence of Bendover Scales*

The values of parallel and perpendicular bendover scales are not fully understood at present, although most indications would suggest that $l_{\rm slab} \geq l_{\rm 2D}$. There are indications from laboratory experiments, such as Robinson & Rusbridge (1971), that the parallel correlation scale may be much larger (∼10 times) than the perpendicular scale in an evolving magnetofluid plasma. This issue is also related to the dynamical development of anisotropy (Shebalin et al. 1983; Oughton et al. 1994) in which shorter correlation scales in the perpendicular direction appear due to the suppression of spectral transfer along the mean magnetic field.

In Figure 6 we show the parallel mean free path for different values of the ratio $\rho = l_{\rm slab}/l_{\rm 2D}$. For equal bendover scales ($\rho = 1$) and for $\rho = 10$, which is the expected value, the theoretical parallel mean free path agrees with the Palmer observations. The importance of the parameter ρ indicates that the two-dimensional contribution to the pitch-angle Fokker-Planck coefficient is important and cannot be neglected. This matter is further discussed in § 5.6. Figure 7 shows the ρ-dependence of the ratio $\lambda_\perp/\lambda_\parallel$.

5.5. *Comparison with the Damping Model of Dynamical Turbulence*

Here we compare NADT results with the parallel mean free path calculated within the DT model proposed by Bieber et al. (1994). For the calculations of the parallel mean free path within

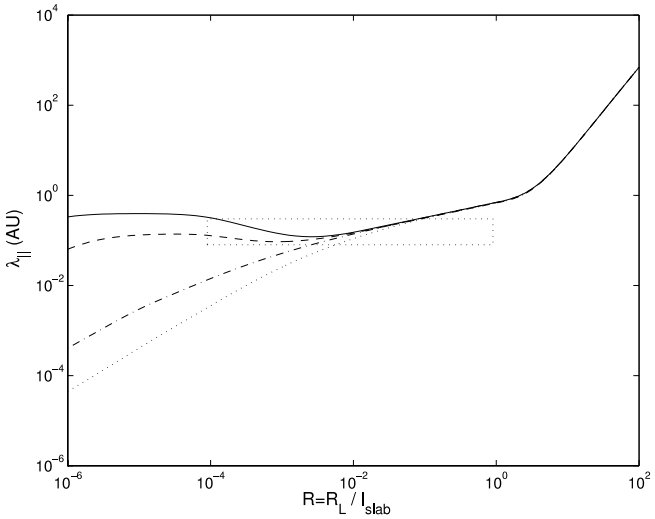

FIG. 6.—Parallel mean free path $\lambda_\parallel$ for different values of $\rho = l_{\rm slab}/l_{\rm 2D}$. We employed QLT to compute the mean free path for electrons with $\rho = 1$ (*solid line*), electrons with $\rho = 10$ (*dashed line*), protons with $\rho = 1$ (*dash-dotted line*), and protons with $\rho = 10$ (*dotted line*).

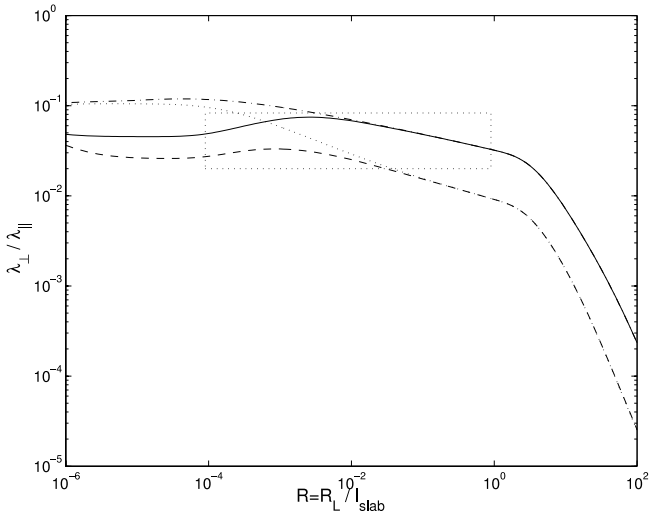

FIG. 7.—Ratio $\lambda_\perp/\lambda_\parallel$ for different values of $\rho = l_{slab}/l_{2D}$. We employed NLGC theory to compute the mean free path for electrons with $\rho = 1$ (*solid line*), electrons with $\rho = 10$ (*dashed line*), protons with $\rho = 1$ (*dash-dotted line*), and protons with $\rho = 10$ (*dotted line*).

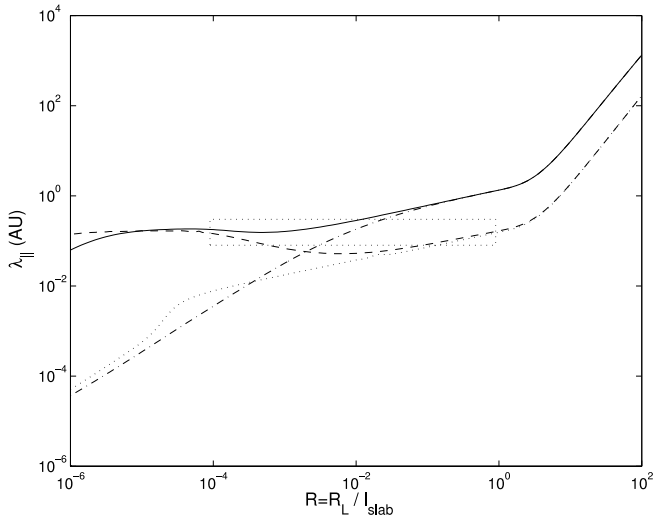

FIG. 9.—Parallel mean free path $\lambda_\parallel$ for different turbulence geometries. Shown are QLT results for electrons with $\delta B^2_{slab}/B^2_0 = 0.1$ (*solid line*), electrons with $\delta B^2_{slab}/B^2_0 = 0.9$ (*dashed line*), protons with $\delta B^2_{slab}/B^2_0 = 0.1$ (*dash-dotted line*), and protons with $\delta B^2_{slab}/B^2_0 = 0.9$ (*dotted line*).

the damping model, we used the analytical results for the pitch-angle Fokker-Planck coefficients of Teufel & Schlickeiser (2003) and Shalchi & Schlickeiser (2004b). Using equation (14), the calculations of the parallel mean free path were done numerically to achieve a higher accuracy. As shown in Figure 8, the DT model provides results that are different from the NADT model. To obtain the DT results, the parameter α (see Table 1) was assumed to be 1.

5.6. *Influence of the Turbulence Geometry*

Here we consider diffusion coefficients for nearly pure slab (90% slab/10% two-dimensional) and nearly pure two-dimensional (10% slab/90% two-dimensional) geometry to explore the importance of the turbulence geometry. First we note that the NADT results are sensitively dependent on the ratio $\delta B_{slab}/\delta B_{2D}$, as shown in Figure 9. Furthermore, we repeated nearly all calculations of the current paper with the two-dimensional pitch-angle Fokker-Planck coefficient neglected, and we found that both Fokker-Planck coefficients are important. The turbulence geometry has an influence in two different ways:

1. The correlation time of the NADT model is dependent on the ratio $\delta B_{2D}/B_0$ (see eq. [12]).
2. The total Fokker-Planck coefficient is a superposition of the slab and the two-dimensional contribution and is therefore dependent on $\delta B^2_{slab}/B^2_0$ and $\delta B^2_{2D}/B^2_0$.

It is an important result of the current paper that neither effect can be neglected. Furthermore, the "bump" for the proton results in the nearly pure slab model comes from the plasma wave dispersion relation. This is the only case for which we found an significant influence of plasma wave effects within the NADT model.

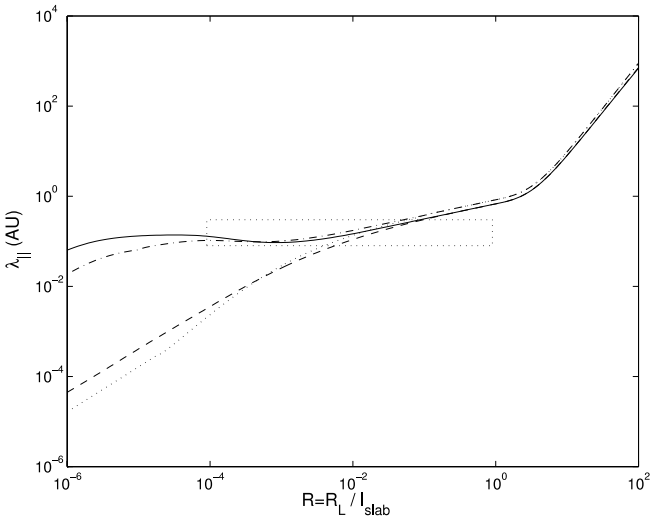

FIG. 8.—Comparison of NADT results for electrons (*solid line*) and protons (*dashed line*) with results of the DT model (Bieber et al. 1994) for electrons (*dash-dotted line*) and protons (*dotted line*).

6. INFLUENCE OF NONLINEAR EFFECTS

In some cases QLT is not appropriate for describing cosmic-ray transport, as shown by numerical test particle simulations (Qin et al. 2002a, 2002b). According to Shalchi (2005b) there are three major problems of cosmic-ray transport: the 90° problem, the geometry problem, and the perpendicular diffusion problem. In turn we consider each of these problems separately to discuss the importance of nonlinear effects. These discussions can give us a hint of how important nonlinear effects are and how reliable the results of the current paper are.

6.1. *The 90° Problem*

It has been discussed in previous papers (e.g., Völk 1973, 1975; Jones et al. 1973, 1978; Goldstein 1976; Shalchi 2005b) that QLT disagrees with magnetostatic slab results obtained from numerical test particle simulations for pitch angles close to 90° ($\mu \approx 0$). Therefore, a nonlinear description of cosmic-ray transport is necessary. According to Goldstein (1976), resonance-broadening effects are the most important nonlinear effects for pitch angles close to 90°, which was confirmed by second-order QLT calculations done by Shalchi (2005b). Such nonlinear extensions are mathematically very similar to the resonance broadening caused by the dynamical effects considered in the current paper. Therefore, one could argue that there is a competition between nonlinear and dynamical turbulence effects for small values

of μ. It should be emphasized that this similarity is of a mathematical nature; the physical meaning is quite different.

Because the magnetostatic second-order parallel mean free path (see Shalchi 2005b) is much larger than the dynamical quasi-linear mean free path calculated in the current paper, it seems that nonlinear effects at 90° can be neglected in comparison with dynamical effects. It must be the subject of future work to prove this statement. One possibility to accomplish such a proof is the application of second-order QLT to the NADT model. Furthermore, test particle simulations in dynamical turbulence could definitely allow investigation of the importance of nonlinear effects in more realistic turbulence models. Previous simulations have been restricted to static turbulence.

6.2. *The Geometry Problem*

It was demonstrated in Shalchi et al. (2004b) that perpendicular diffusion itself could have a strong influence on pitch-angle diffusion because it also generates resonance broadening. A theory that takes into account such effects was already derived and is called WNLT (Shalchi et al. 2004b). In general WNLT calculations could also be done within dynamical turbulence models, but such calculations are extremely tedious, and we leave such an investigation for future work.

It should be noted that this nonlinear effect, which arises because of the coupling between parallel and perpendicular transport, is strongly parameter dependent. If we assume equal length scales ($l_{2D} = l_{slab}$), the quasi-linear parallel mean free path is close to the upper limit of the Palmer box (see Fig. 6). In this case the nonlinear effects that are neglected in QLT can decrease the parallel mean free path, so that we achieve agreement with the Palmer consensus. In the other extreme case, namely, $l_{2D} \ll l_{slab}$, the QLT parallel mean free path is already close to the lower limit of the Palmer consensus. In addition, nonlinear effects are very strong for small values of the two-dimensional bendover scale (see Shalchi et al. 2004b) and make the parallel mean free path even smaller. In this case we can no longer reproduce the observations. Therefore, three steps are essential for the near future:

1. An accurate measurement of the ratio l_{2D}/l_{slab} should be made. As demonstrated in the current paper, this ratio is one of the key input parameters into transport theories, especially if a nonlinear theory is applied.
2. A calculation of the parallel diffusion coefficient within a nonlinear theory has to be done within dynamical turbulence.
3. Numerical test particle simulations have to be done within the NADT model to investigate the influence of nonlinear effects in realistic turbulence models.

6.3. *The Perpendicular Diffusion Problem*

As noted in Matthaeus et al. (2003) and Shalchi et al. (2004b), a nonlinear description of perpendicular transport is essential. NLGC theory and WNLT have shown agreement with numerical test particle simulations. Whereas WNLT does not use some of the approximations of the NLGC formulation (e.g., neglecting the gyromotion of the particle), NLGC theory is more tractable than WNLT. In the current paper we only consider the NLGC approach because of its better applicability.

It should be noted, however, that WNLT and NLGC are based on models (Gaussian statistics, exponential form of the velocity correlation function, diffusion *Ansatz*) that could become incorrect for certain parameter regimes. So far the only case in which a disagreement between these new theories and simulations was discovered is that for pure magnetostatic slab geometry, in which perpendicular transport is subdiffusive (see, e.g., Qin et al. 2002a, 2002b; Shalchi 2005a), which cannot be described by WNLT or NLGC theory. The reason for the invalidity of both theories for slab geometry is that the velocity correlation function has a non-exponential tail as described in Kóta & Jokipii (2000) and Shalchi (2005a), which was not included in both these approaches.

QLT is not appropriate for describing perpendicular transport. This statement can be justified by at least three arguments:

1. In the magnetostatic limit QLT shows diffusion for pure slab geometry (Jokipii 1966; Forman et al. 1974; Shalchi 2005a) and superdiffusion for the composite model (Shalchi & Schlickeiser 2004a), which disagrees with numerical test particle simulations in which we find subdiffusion for pure slab and diffusion for composite geometry. If QLT would be the correct theory for perpendicular transport, it would provide the correct results for the magnetostatic model.
2. In Shalchi & Schlickeiser (2004a) the quasi-linear perpendicular mean free path was calculated for the DT model. There it was demonstrated that for heliospheric parameters (e.g., $\delta B/B_0 \sim 1$), the ratio $\lambda_\perp/\lambda_\parallel$ reaches extremely large values ($\lambda_\perp/\lambda_\parallel \sim 10^3$), which disagrees with observations (e.g., Palmer 1982; Dwyer et al. 1997; Zhang et al. 2003; Bieber et al. 2004).
3. QLT uses unperturbed orbits and therefore fails to take into account the effect of parallel scattering on the particles' attempt to follow field lines. For most parameters we expect that perpendicular scattering occurs on much larger timescales than parallel scattering. Therefore, the assumption of unperturbed orbits seems to be inappropriate if the perpendicular mean free paths are calculated.

7. SUMMARY AND CONCLUSION

In this paper we revisit the Palmer consensus. We employ the quasi-linear approximation and the nonlinear guiding center theory to calculate the mean free paths within the new NADT model for the dynamical correlation function. A comparison with observations is presented. We come to the following conclusions:

1. Observed diffusion coefficients in the heliosphere can be explained by the NADT model.
2. Within the NADT model we can no longer neglect the two-dimensional pitch-angle Fokker-Planck coefficient. Both the slab and two-dimensional contributions to pitch-angle scattering are important.
3. A nonlinear description of perpendicular transport is necessary. It is argued in the current paper that QLT is not valid for transport perpendicular to a background magnetic field. For parallel transport, nonlinear effects can also be important depending on the turbulence parameters.
4. If the NADT model is an accurate turbulence model, we can neglect the contribution of the plasma wave dispersion relation to particle diffusion for most parameter regimes. Such effects are small in comparison to dynamical turbulence effects.
5. The DT model that was considered in Bieber et al. (1994) and Dröge (2000) provides similar results for certain parameter regimes but disagrees in general with the NADT model.
6. It is demonstrated that the ratio of the bendover scales l_{slab}/l_{2D} has a strong influence on the parallel mean free path. In addition, the importance of nonlinear effects is strongly dependent on this ratio. An accurate determination of this ratio by observations would be an important step in heliospheric cosmic-ray physics.
7. To draw a final conclusion regarding the importance of nonlinear effects for parallel transport, numerical test particle simulations have to be done in dynamical turbulence.

Within the NADT model in combination with QLT and NLGC theory, we are, in principle, able to explain observed diffusion coefficients in the heliosphere. On the other side we can reproduce numerical test particle simulations only within recently proposed nonlinear theories for parallel transport. From simulations and these new theories, we learn that nonlinear effects are also important for parallel transport. Therefore the new, nonlinear theories must be combined with the NADT model to study the accuracy of QLT for parallel transport in dynamical turbulence. Furthermore, it is important to explore the importance of plasma wave damping effects and electric fields. Such an investigation is a subject of future work.

This work is the result of a collaboration between the Bartol Research Institute, University of Delaware, and the University of Bochum, Theoretische Physik IV. This research was supported by the National Science Foundation under grants ATM-0000315 and ATM-010254 and by NASA under grants NAG5-11603 and NAG5-8134. Furthermore, we acknowledge support by Deutsche Forschungsgemeinschaft through Sonderforschungsbereich 591.

APPENDIX

ANALYTICAL APPROXIMATION OF $\tilde{D}_{\mu\mu}^{\rm slab}$

According to equation (27), the slab pitch-angle Fokker-Planck coefficient has the form

$$\tilde{D}_{\mu\mu}^{\rm slab} = \frac{C(\nu)(1-\mu^2)}{R}\frac{\delta B_{\rm slab}^2}{B_0^2}(1-\mu\epsilon)^2\frac{\beta}{\Omega}I(\beta/\Omega, R(\mu-\epsilon)), \tag{A1}$$

with

$$I(\beta/\Omega, R(\mu-\epsilon)) = \int_0^\infty dx\, h^{\rm slab}(x)\sum_{n=\pm1}\frac{1}{(\beta/\Omega)^2+[xR(\mu-\epsilon)+n]^2}. \tag{A2}$$

For the wave spectrum of equation (26) we find

$$\begin{aligned} I(\beta/\Omega, R(\mu-\epsilon)) \approx & \int_0^1 dx\sum_{n=\pm1}\frac{1}{(\beta/\Omega)^2+[xR(\mu-\epsilon)+n]^2} + \int_1^\infty dx\sum_{n=\pm1}\frac{x^{-s}}{(\beta/\Omega)^2+[xR(\mu-\epsilon)+n]^2} \\ & - \int_{\xi_{\rm slab}}^\infty dx\sum_{n=\pm1}\frac{x^{-s}}{(\beta/\Omega)^2+[xR(\mu-\epsilon)+n]^2} + \xi_{\rm slab}^{p-2\nu}\int_{\xi_{\rm slab}}^\infty dx\sum_{n=\pm1}\frac{x^{-p}}{(\beta/\Omega)^2+[xR(\mu-\epsilon)+n]^2}, \end{aligned} \tag{A3}$$

where we used the spectral index $s = 2\nu$. For the last two integrals we apply the transformation $x \to x/\xi_{\rm slab}$ to find

$$I(\beta/\Omega, R(\mu-\epsilon)) = A(\beta/\Omega, R(\mu-\epsilon)) + B(\beta/\Omega, R(\mu-\epsilon), s) - \xi_{\rm slab}^{1-s}B(\beta/\Omega, R\xi_{\rm slab}(\mu-\epsilon), s) + \xi_{\rm slab}^{1-s}B(\beta/\Omega, R\xi_{\rm slab}(\mu-\epsilon), p), \tag{A4}$$

with the two integrals

$$\begin{aligned} A(a,b) &= \int_0^1 dx\left[\frac{1}{a^2+(bx+1)^2}+\frac{1}{a^2+(bx-1)^2}\right], \\ B(a,b,s) &= \int_1^\infty dx\left[\frac{x^{-s}}{a^2+(bx+1)^2}+\frac{x^{-s}}{a^2+(bx-1)^2}\right]. \end{aligned} \tag{A5}$$

Here a is a positive real number, whereas b can be positive or negative. The integral A can be solved, and we obtain

$$A(a,b) = \frac{\arctan[(b+1)/a]+\arctan[(b-1)/a]}{ab}. \tag{A6}$$

The integral B is considered below.

A1. THE INTEGRAL $B(A, B, S)$

The integral B can be written as

$$B(a,b,s) = \frac{1}{b^2}\int_1^\infty dx\left[\frac{x^{-s}}{(x+\alpha_1)(x+\alpha_2)}+\frac{x^{-s}}{(x+\alpha_3)(x+\alpha_4)}\right], \tag{A7}$$

with

$$\alpha_1 = \frac{+1 + ia}{b},$$
$$\alpha_2 = \frac{+1 - ia}{b},$$
$$\alpha_3 = \frac{-1 + ia}{b},$$
$$\alpha_4 = \frac{-1 - ia}{b}. \tag{A8}$$

The function B can be further simplified to

$$B(a,b,s) = \frac{i}{2ab}\left(\int_1^\infty dx\,\frac{x^{-s}}{x+\alpha_1} - \int_1^\infty dx\,\frac{x^{-s}}{x+\alpha_2} + \int_1^\infty dx\,\frac{x^{-s}}{x+\alpha_3} - \int_1^\infty dx\,\frac{x^{-s}}{x+\alpha_4}\right). \tag{A9}$$

According to Gradshteyn & Ryzhik (2000), these integrals can be expressed by hypergeometric functions,

$$\int_1^\infty dx\,\frac{x^{-s}}{x+\alpha_i} = \frac{1}{s}\,{}_2F_1(1,s,s+1;-\alpha_i), \tag{A10}$$

and we therefore obtain

$$B(a,b,s) = \frac{i}{2sab}\left[{}_2F_1(1,s,s+1;-\alpha_1) - {}_2F_1(1,s,s+1;-\alpha_2)\right] + \left[{}_2F_1(1,s,s+1;-\alpha_3) - {}_2F_1(1,s,s+1;-\alpha_4)\right]. \tag{A11}$$

In turn we discuss this formula for different cases.

A2. THE CASE $b^2 \gg a^2 + 1$

Here the $\mid \alpha_i \mid$ are small numbers, and we can approximate the hypergeometric functions by (see, e.g., Abramowitz & Stegun 1974)

$${}_2F_1(1,s,s+1;-\alpha_i) \approx 1 + \frac{s}{s+1}\,\alpha_i. \tag{A12}$$

Combining this result with equations (A8) and (A11), we obtain

$$B(b^2 \gg a^2 + 1, s) \approx \frac{2}{(s+1)}\,\frac{1}{b^2}, \tag{A13}$$

which is the final result of this subsection.

A3. THE CASE $b^2 \ll a^2 + 1$

In this case the $\mid \alpha_i \mid$ are large numbers, and we must apply the formula (see, e.g., Abramowitz & Stegun 1974),

$${}_2F_1(a,b;c;z) = \frac{\Gamma(c)\Gamma(b-a)}{\Gamma(b)\Gamma(c-a)}(-z)^{-a}\,{}_2F_1\left(a,a+1-c;a+1-b;\frac{1}{z}\right) + \frac{\Gamma(c)\Gamma(a-b)}{\Gamma(a)\Gamma(c-b)}(-z)^{-b}\,{}_2F_1\left(b,b+1-c;b+1-a;\frac{1}{z}\right), \tag{A14}$$

[if $|\arg(-z)| < \pi$ and $a - b \neq 0, \pm 1, \pm 2, \ldots$] to find

$${}_2F_1(1,s,s+1;-\alpha_i) = \frac{\Gamma(s+1)\Gamma(s-1)}{\Gamma(s)\Gamma(s)}(-\alpha_i)^{-1}\,{}_2F_1\left(1,1-s;2-s;\frac{1}{\alpha_i}\right) + \frac{\Gamma(s+1)\Gamma(1-s)}{\Gamma(1)\Gamma(1)}(-\alpha_i)^{-s}\,{}_2F_1\left(s,0;s;\frac{1}{\alpha_i}\right). \tag{A15}$$

By using $\Gamma(1) = 1$, $\Gamma(x+1) = x\Gamma(x)$, ${}_2F_1(s,0;s;1/\alpha_i) = 1$, and by approximating the first hypergeometric function as done in equation (A12), we obtain

$${}_2F_1(1,s,s+1;-\alpha_i) \approx \frac{s}{1-s}\,\frac{1}{\alpha_i} + \frac{\pi s}{\sin(\pi s)}\left(\frac{-1}{\alpha_i}\right)^s. \tag{A16}$$

In combination with equation (A11), we find

$$B(b^2 \ll a^2+1,s) \approx \frac{2}{(s-1)(1+a^2)} + \frac{i\pi}{2a\sin(\pi s)}|b|^{s-1}E(a,s), \tag{A17}$$

where we used

$$E(a,s) = (1+a^2)^{-s}[(+1-ia)^s - (+1+ia)^s + (-1-ia)^s - (-1+ia)^s]. \tag{A18}$$

The function E must be considered for two different cases.

A3.1. *The Case* $a \ll 1$

Here we have

$$\begin{aligned}[(+1 \pm ia)^s]_{a\to 0} &\to 1,\\ [(-1+ia)^s]_{a\to 0} &\to (-1)^s = e^{s\ln(-1)} = e^{+i\pi s},\\ [(-1-ia)^s]_{a\to 0} &\to [(-1)^s]^* = e^{-i\pi s},\end{aligned} \tag{A19}$$

and we find

$$E(a\ll 1,s) \approx 1 - 1 + e^{-i\pi s} - e^{+i\pi s} = \frac{2}{i}\sin(\pi s); \tag{A20}$$

therefore,

$$B(b^2 \ll a^2+1, a\ll 1, s) \approx \frac{2}{(s-1)(1+a^2)} + \frac{\pi}{a}|b|^{s-1}. \tag{A21}$$

A3.2. *The Case* $a \gg 1$

Here we find (note that a is a positive number)

$$E(a\gg 1,s) \sim O\left(\frac{1}{a^s}\right), \tag{A22}$$

and therefore,

$$\begin{aligned}B(b^2 \ll a^2+1, a\gg 1, s) &\approx \frac{2}{(s-1)(1+a^2)} + \frac{\pi}{a}|b|^{s-1}O\left(\frac{1}{a^s}\right)\\ &\approx \frac{2}{(s-1)(1+a^2)} + \frac{\pi}{a^2}O\left(\frac{|b|^{s-1}}{a^{s-1}}\right).\end{aligned} \tag{A23}$$

In the case considered here we have $b^2 \ll a^2$, and we always assume $s > 1$. Therefore, we have

$$B(b^2 \ll a^2+1, a\gg 1, s) \approx \frac{2}{(s-1)(1+a^2)}. \tag{A24}$$

A4. SUMMARY

We derived the following three cases for the function B,

$$\begin{aligned}B(b^2 \gg a^2+1,s) &\approx \frac{2}{(s+1)}\frac{1}{b^2},\\ B(b^2 \ll a^2+1, a\ll 1, s) &\approx \frac{2}{(s-1)(1+a^2)} + \frac{\pi}{a}|b|^{s-1},\\ B(b^2 \ll a^2+1, a\gg 1, s) &\approx \frac{2}{(s-1)(1+a^2)}.\end{aligned} \tag{A25}$$

Together with equations (A1), (A4), and (A6), we can simplify the slab pitch-angle Fokker-Planck coefficient $D_{\mu\mu}$. By applying the methods presented in Teufel & Schlickeiser (2002, 2003), it would be straightforward to derive analytical results for $D_{\mu\mu}$ and $\lambda_\parallel$. In the current paper the focus is more on a comparison between theory and observations, and we therefore abstain from such time-consuming analytical calculations.

REFERENCES

Abramowitz, M., & Stegun, I. A. 1974, Handbook of Mathematical Functions (New York: Dover)
Bavassano, B. 2003, in AIP Conf. Proc. 679, Solar Wind Ten, ed. M. Velli et al. (New York: AIP), 377
Bieber, J. W., & Matthaeus, W. H. 1997, ApJ, 485, 655
Bieber, J. W., Matthaeus, W. H., Shalchi, A., & Qin, G. 2004, Geophys. Res. Lett., 31, L10805
Bieber, J. W., Wanner, W., & Matthaeus, W. H. 1996, J. Geophys. Res., 101, 2511
Bieber, J. W., et al. 1994, ApJ, 420, 294
Burger, R. A., Potgieter, M. S., & Heber, B. 2000, J. Geophys. Res., 105, 27447
Chenette, D. L., Conlon, T. F., Pyle, K. R., & Simpson, J. A. 1977, ApJ, 215, L95
Dröge, W. 2000, ApJ, 537, 1073
Dwyer, J. R., et al. 1997, ApJ, 490, L115
Earl, J. A. 1974, ApJ, 193, 231
Forman, M. A., Jokipii, J. R., & Owens, A. J. 1974, ApJ, 192, 535
Giacalone, J., & Jokipii, J. R. 1999, ApJ, 520, 204
Gloeckler, G., Schwadron, N. A., Fisk, L. A., & Geiss, J. 1995, Geophys. Res. Lett., 22, 2665
Goldreich, P., & Sridhar, S. 1995, ApJ, 438, 763
Goldstein, M. L. 1976, ApJ, 204, 900
Gradshteyn, I. S., & Ryzhik, I. M. 2000, Table of Integrals, Series, and Products (6th ed.; San Diego: Academic Press)
Hasselmann, K., & Wibberenz, G. 1968, Z. Geophys., 34, 353
Jokipii, J. R. 1966, ApJ, 146, 480
Jones, F. C., Birmingham, T. J., & Kaiser, T. B. 1973, ApJ, 180, L139
———. 1978, Phys. Fluids, 21, 347
Kóta, J., & Jokipii, J. R. 2000, ApJ, 531, 1067
Matthaeus, W. H., Goldstein, M., & Roberts, D. A. 1990, J. Geophys. Res., 95, 20673
Matthaeus, W. H., et al. 2003, ApJ, 590, L53
Michalek, G., & Ostrowski, M. 1996, Nonlinear Processes Geophys., 3, 66
Möbius, E., Rucinski, D., Lee, M. A., & Isenberg, P. A. 1998, J. Geophys. Res., 102, 257
Oughton, S., Matthaeus, W. H., & Dmitruk, P. 2006, Phys. Plasmas, in press
Oughton, S., Priest, E., & Matthaeus, W. H. 1994, J. Fluid Mech., 280, 95
Palmer, I. D. 1982, Rev. Geophys. Space Phys., 20, 335
Qin, G., Matthaeus, W. H., & Bieber, J. W. 2002a, ApJ, 578, L117
———. 2002b, Geophys. Res. Lett., 29, 7-1
———. 2006, ApJ, 640, L103
Reames, D. V. 1999, Space Sci. Rev., 90, 413
Robinson, D. C., & Rusbridge, M. G. 1971, Phys. Fluids, 14, 2499
Schlickeiser, R., 2002, Cosmic Ray Astrophysics (Berlin: Springer)
Shalchi, A. 2005a, J. Geophys. Res., 110, A09103
———. 2005b, Phys. Plasmas, 12, 052905
———. 2006, A&A, 448, 809
Shalchi, A., Bieber, J. W., Matthaeus, W. H., & Qin, G. 2004a, ApJ, 615, 805
———. 2004b, ApJ, 616, 617
Shalchi, A., & Schlickeiser, R. 2004a, A&A, 420, 821
———. 2004b, ApJ, 604, 861
Shebalin, J. V., Matthaeus, W. H., & Montgomery, D. 1983, J. Plasma Phys., 29, 525
Teufel, A., & Schlickeiser, R. 2002, A&A, 393, 703
———. 2003, A&A, 397, 15
Tu, C.-Y., & Marsch, E. 1993, J. Geophys. Res., 98, 1257
Völk, H. J. 1973, Ap&SS, 25, 471
———. 1975, Rev. Geophys. Space Phys., 13, 547
Zhang, M., Jokipii, J. R., & McKibben, R. B. 2003, ApJ, 595, 493
Zhou, Y., Matthaeus, W. H., & Dmitruk, P. 2004, Rev. Mod. Phys., 76, 1015